Improved Binding of Cytochrome P450cam Substrate Analogues Designed To Fill Extra Space in the Substrate Binding Pocket†

Volkhard Helms,‡ Eric Deprez,§ Edward Gill,|| Christel Barret,§ Gaston Hui Bon Hoa,§ and Rebecca C. Wade*,‡

European Molecular Biology Laboratory, Meyerhofstrasse 1, 69012 Heidelberg, Germany, INSERM Unité 310, Institut de Biologie Physico-Chimique, 13, rue Pierre et Marie Curie, 75005 Paris, France, and Department of Pharmacology, University of Oxford, Oxford OX1 3QT, England

Received August 4, 1995; Revised Manuscript Received November 20, 1995⊗

ABSTRACT: Cytochrome P450cam catalyzes the 5-*exo*-hydroxylation of camphor. Camphor analogues were designed to fill an empty region of the substrate binding pocket with the expectation that they would bind more tightly than camphor itself due to increased van der Waals interactions with the protein and the displacement of any solvent occupying this site. A series of compounds (*endo*-borneol methyl ether, *endo*-borneol propyl ether, *endo*-borneol allyl ether and *endo*-borneol dimethyl allyl ether) were synthesized with substituents at the camphor carbonyl oxygen. The spin conversion and thermodynamic properties of this series of compounds were measured for wild type and Y96F mutant cytochrome P450cam and were interpreted in the context of molecular dynamics simulations of the camphor analogues in the P450 binding site and in solution. Compounds with a 3-carbon chain substituent were predicted to match the size of the unoccupied region most optimally and thus bind best. Consistent with this prediction, the borneol allyl ether binds to cytochrome P450cam with highest affinity with a $K_d = 0.6 \pm 0.1$ μM (compared to a $K_d = 1.7 \pm 0.2$ μM for camphor under the same experimental conditions). Binding of the camphor analogues to the Y96F mutant is much enhanced over the binding of camphor, indicating that hydrogen bonding plays a less important role in binding of these analogues. Binding enthalpies calculated from the simulations, taking all solvent contributions into account, agree very well with experimental binding enthalpies. Binding affinity is not however correlated with the calculated binding enthalpy because the binding of the substrate analogues is characterized by enthalpy−entropy compensation. The new compounds are useful probes for further studies of the mechanism of cytochrome P450cam due to their high binding affinities and high spin properties.

In the past few years, the ability to design ligands to bind strongly and very specifically to a target protein, as either substrates or inhibitors, has improved considerably due to the availability of an increasing number of three-dimensional structures of proteins and their complexes with ligands, the improvement of computing resources, and the development of new structure based modeling techniques (Appelt *et al*., 1991; Kuntz, 1992; Navia & Murcko, 1992; Shoichet *et al*., 1993; Colman, 1994; Greer *et al*., 1994; Pisabarro *et al*., 1994; De Voss & Ortiz de Montellano, 1995). The aim of this work is to examine the value of designing ligand modifications to fill empty space in ligand binding sites in proteins for obtaining improved binding affinity.

Evidence from protein stability studies shows that the introduction of cavities into proteins by mutating hydrophobic residues to ones with smaller side chains is destabilizing (Eriksson *et al*., 1992a; Serrano *et al*., 1992). On the other hand, it is sometimes possible for a cavity introduced by a single point mutation to be filled by a small compound that binds specifically and stabilizes the protein. For example, a benzene molecule binds in the hole created by a Leu → Ala mutation in T4 lysozyme and stabilizes the enzyme (Eriksson *et al*., 1992b), and substituted imidazoles bind in a cavity created by a Trp → Gly mutation in cytochrome *c* peroxidase (Fitzgerald *et al*., 1994). The effect of adding a hydrocarbon amino acid side chain of increasing length to a peptide ligand to occupy a pocket on the surface of a set of serine proteases was analyzed by Bigler *et al.* (1993). Measurements of association constants indicate that the optimum side chain length for binding is different for the different proteases and that binding free energy differences are dependent on whether the protein is distorted by the ligand. Our focus here is on the effect of adding a hydrocarbon chain of chosen length and rigidity on the binding characteristics of a small nonpeptidic predominantly nonpolar ligand.

Polar ligands generally bind either on protein surfaces or at sites that are directly solvent-accessible, e.g., sialic acid to influenza virus hemagglutinin (Weis *et al.*, 1988) and neuraminidase (Varghese *et al.*, 1992; Burmeister *et al*., 1992), and peptides to the MHC protein (Fremont *et al*., 1992). On the other hand, predominantly nonpolar ligands often bind in buried cavities, e.g., the antiviral WIN compounds to rhinovirus (Badger *et al*., 1988), and camphor in cytochrome P450cam (Poulos *et al*., 1987). In this paper, we describe a study of the binding of nonpolar compounds using cytochrome P450cam as a well-characterized test system. Specifically, substrate analogues were designed on the basis of the structure of the protein−substrate binary complex to bind more strongly to cytochrome P450cam than

† This work was supported in part by the EU Biotechnology Programme (BIO2-CT94-2060).

‡ European Molecular Biology Laboratory.

§ INSERM Unité 310.

|| University of Oxford.

⊗ Abstract published in *Advance ACS Abstracts,* January 15, 1996.

0006-2960/96/0435-1485$12.00/0

the natural substrate, camphor, by filling space in the binding site. Cytochrome P450cam is well suited for molecular design studies because the structures of the substrate-free and camphor-bound protein are almost identical and the active site is not directly accessible to the solvent; these properties facilitate the identification of solvent involved in binding. However, it is clearly not straightforward to design compounds to bind better than camphor to P450cam; e.g., De Voss and Ortiz de Montellano (1995) only identified compounds that bind with lower affinity using the DOCK program.

In this paper, we consider the binding of the new camphor analogues with specific regard to the roles of shape complementarity, hydrogen bonds, entropy, and solvent.

Shape Complementarity. One of the tenets of the successful design of potent inhibitors and the improvement of the binding properties of naturally observed ligands is the concept of shape complementarity between the ligand and the protein binding site (Kuntz *et al*., 1982; Cherfils & Janin, 1993). Maximizing shape complementarity implies optimizing van der Waals interactions between the protein and the ligand, displacing solvent from the interface, and minimizing the volume of any interfacial cavities. It is the guiding principle for the design of the camphor analogues studied in this paper.

Hydrogen Bonds. Protein−ligand hydrogen bonds are important for binding specificity. One strategy for designing protein−ligand interactions is to satisfy all the hydrogen bonding capacity at the protein−ligand interface. However, a ligand that makes a hydrogen bond with a protein group will not always bind better to the protein than a ligand that cannot because of differences in the desolvation energies of the ligands (Fersht *et al*., 1985). Here, the design of camphor analogues to improve shape complementarity requires alteration, with respect to camphor, of the strength of the compound's hydrogen bond to the protein.

Enthalpy-Entropy Compensation. The phenomenon of enthalpy−entropy compensation is a characteristic feature of hydrophobic interactions in aqueous solution and has long been observed in a variety of biological processes, such as protein folding and the binding of nonpolar ligands to proteins (Lumry & Rajender, 1970). The solvation of nonpolar molecules (hydrophobic hydration) has been found to involve a slightly negative enthalpy change and a significant decrease in entropy (Tanford, 1973). "Hydrophobic interaction" refers to the solvent-induced forces that drive nonpolar solutes together when in an aqueous environment (Kauzmann, 1959). Such association is entropically favorable due to the overall reduction in solvent-exposed nonpolar surface. This solvent entropy-based interpretation is, e.g., supported by computer simulations examining the temperature dependence of the aggregation of ethane in aqueous solution (Mancera & Buckingham, 1995). The underlying fundamentals of the hydrophobic effect and therefore the principles governing the interaction of proteins and hydrophobic ligands are, however, still controversial; see, e.g., Chan and Dill (1994) or Jackson and Sternberg (1994).

Aqueous Solvent. Empty ligand binding sites are usually filled by solvent molecules which are either fully or partly released upon binding of the ligand, with a concomitant favorable gain in translational entropy. Such water molecules can be located by X-ray (Saenger, 1987) and neutron diffraction (Savage, 1993) if they are spatially ordered and by nuclear magnetic resonance if they have long residence times (Otting *et al*., 1991). They have been observed in both polar and nonpolar protein cavities (Ernst *et al*., 1995) and binding sites. For example, upon binding of biotin and HABA to streptavidin, all five water molecules are observed to be displaced from the active site (Weber *et al*., 1992). In the complex of endothiapepsin and a peptidic inhibitor (Sali *et al*., 1989), 23 ordered water molecules are displaced upon binding and 7 ordered water molecules remain in the active site. Such water molecules often mediate hydrogen bonds between the protein and the ligand, e.g., in the complexes of sugar binding proteins with sugars (Quiocho, 1991) and in the complex of 6-deoxyerythronolide B with cytochrome P450eryF (Cupp-Vickery & Poulos, 1995). Water molecules can also be displaced by the introduction of a hydroxyl moiety; e.g., the mutation of Ala → Ser in a neutral protease excluded an ordered water molecule from the protein interior (Vriend *et al*., 1991) and increased the protein stability. In this study, we discuss the hydration of the space filled by the camphor analogues and the merits of displacing solvent from it.

Cytochrome P450cam. The family of cytochrome P450 heme proteins catalyzes many different reactions on predominantly hydrophobic substrates. Members of the family are ubiquitous in biological systems where they play important roles in the synthesis of steroids and fatty acids, and in the metabolism of xenobiotics (Guengerich, 1991). Cytochrome P450cam from the bacterium *Pseudomonas putida* has been studied in great detail by a variety of methods, including crystallography (Poulos & Raag, 1992), spectroscopy (Schulze *et al*., 1994), site-directed mutagenesis (Sligar *et al*., 1991), application of osmotic and hydrostatic pressure (Di Primo *et al*., 1995), photoacoustic calorimetry (Di Primo *et al*., 1993), and computer modeling (Baldwin *et al.*, 1991) and simulation (see Harris and Loew (1995), Jones *et al*. (1995), and Loida *et al*. (1995) and references therein), and serves as a model system for the understanding of other P450s. It catalyzes the regiospecific hydroxylation of its natural substrate, camphor, to 5-*exo*-hydroxycamphor.

There is a considerable amount of experimental data characterizing the binding of ligands to P450cam and the changes in hydration of the active site on binding. In the crystal structure of the ligand-free form of P450cam (Poulos *et al*., 1986), six water molecules were assigned inside the active site. One of them is the sixth (distal) ligand of the iron, and the five others form a cluster connected by hydrogen bonds. The heme Fe spin state is low spin (Tsai *et al*., 1970). In the crystal structures of P450cam with the high affinity substrates camphor and adamantanone, the bound ligands form a strong hydrogen bond with Tyr96 and no water molecules are observed in the active site. The iron spin state in the presence of these ligands is high spin (94% high spin with camphor (Sligar, 1976)). In the crystal structures of complexes with compounds that bind with less affinity, either because they are considerably smaller than camphor, e.g., norcamphor, or because they lack the ability to form a hydrogen bond to Tyr96, e.g., camphane, a water molecule occupies the position of the sixth ligand to Fe (Raag & Poulos, 1991) and the Fe spin has intermediate values (Fisher & Sligar, 1985; Atkins & Sligar, 1988). In the camphor complex of the Y96F mutant, the Fe spin state has an intermediate value of 59% (Atkins and Sligar, 1988). The

iron spin state has been interpreted as an indicator of the water accessibility of the iron and the degree of solvation of the active site (Fisher *et al*., 1985). Thus, the reduced spin in the Y96F mutant has been explained by enhanced mobility of camphor in the active site of Y96F, allowing water molecules to access the heme center (Di Primo *et al*., 1990). In addition to the crystallographically observed water molecules, other less ordered solvent molecules may remain in the active site when the ligands bind, but so far it has not been possible to study the number and location of such water molecules nor their thermodynamic contribution to ligand binding.

The binding of camphor to P450cam is characterized by enthalpy−entropy compensation with a favorable entropy change (Griffin & Peterson, 1972). Because the thermodynamic parameters for camphor binding at 294 K are in the same range as those for the transfer of hydrocarbons from water to nonpolar solvent, it was suggested that the driving force for substrate binding is the favorable entropy of desolvation on transfer of the hydrophobic substrate from an aqueous environment to a hydrophobic region of the protein (Griffin & Peterson, 1972). Crystallographic evidence (Poulos *et al.*, 1986) points to another source of favorable binding entropy, namely, the release of the solvent molecules from the active site upon ligand binding.

Design of Space-Filling Camphor Analogues. In an earlier study (Wade, 1990), the interaction energies of methyl and water probes in the active site of P450cam with the protein were calculated using the GRID program (Goodford, 1985; Boobbyer *et al*., 1989; Wade *et al*., 1993; Wade & Goodford, 1993). The energetically favorable region for a methyl probe in the active site of the structure of the P450cam−camphor complex (camphor was removed from the active site) is shown in Figure 1A. The camphor body is enclosed by the volume accessible to the methyl probe, and only the camphor carbonyl oxygen sticks out from this volume. The total volume of the active site of P450cam with camphor removed was calculated with the GRASP program (Nicholls & Honig, 1991) as 0.300 nm^3. The volume inside camphor's molecular surface is 0.141 nm^3. Therefore, camphor only fills ca. 47% of the active site volume. The methyl probe energy contours show a hydrophobic region next to residues Phe87 and Phe193 that is connected to the camphor volume and is unoccupied by camphor. Wade (1990) suggested that this region could be filled by camphor analogues with a hydrophobic moiety added at the camphor carbonyl position that could make favorable van der Waals contacts with the surrounding residues. The modeled structure of a camphor analogue with a 3-carbon moiety (*endo*-borneol *O*-allyl ether) is shown in Figure 1B.

For the camphor-bound form of P450cam, two energy minima below −24 kJ mol^{-1} were located with the GRID program for a water molecule inside the active site. One of them, which was labeled "site D", is in the region that could be filled by camphor analogues such as that shown in Figure 1B. Although it is located in a hydrophobic region of the active site, the site is within hydrogen bonding distance of the camphor oxygen. Thus, it is not a favorable site for a water probe in the absence of camphor, but in the presence of camphor, a water molecule in this position could donate a hydrogen bond of optimal geometry to the camphor oxygen. Thus, the hydrogen bonding capacity of camphor would be fully satisfied, and the water molecule would

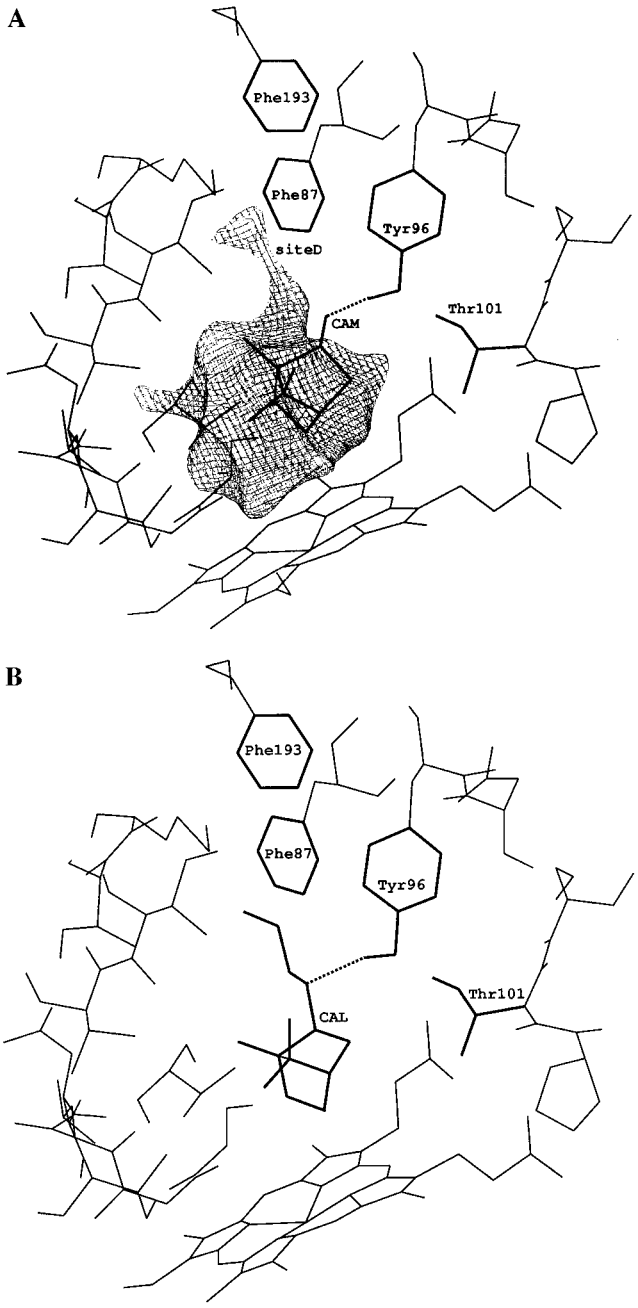

FIGURE 1: Crystal structure of the complex of cytochrome P450cam with camphor: (A) Energy contour at −9.3 kJ mol^{-1} for a methyl probe calculated with the GRID program with camphor removed from the structure. "Site D" is explicitly labeled. (B) A camphor analogue with an allyl ether moiety modeled to fill the space near site D. The dashed line indicates the hydrogen bond with Tyr96.

contribute, along with Tyr96, to stabilizing the binding of camphor in the active site in the correct orientation for the regiospecific reaction. On the other hand, we have recently calculated the hydration free energy of this region by MD[1] simulation (Helms & Wade, 1995) and found it to be unfavorable by +15.8 ± 5.0 kJ mol^{-1}, although transient occupation is possible and was also observed in an MD

[1] Abbreviations: MD, molecular dynamics; LJ, Lennard Jones; NVT, NVE, NPT, indicate which properties are kept constant during an MD simulation: particle number *N*, volume *V*, temperature *T*, or pressure *P*; RMS, root mean square; SASA, solvent-accessible surface area; CAM, camphor; CEN, *endo*-borneol methyl ether; CEP, *endo*-borneol propyl ether; CAL, *endo*-borneol allyl ether; Y96F, mutant of cytochrome P450cam in which Tyr96 is replaced by Phe.

simulation of the complex of P450cam with norcamphor (Harris & Loew, 1995). Occupation of this region by a ligand would result in any water in this region of the active site, whether ordered or disordered, being pushed into the bulk solvent with an accompanying favorable entropy change.

Outline of Paper. In this work, four novel camphor analogues were synthesized, in which the camphor carbonyl group was replaced by an ether oxygen linked to a hydrocarbon tail of varying length. Binding to P450cam was characterized by experimental and theoretical techniques, and in the Results section, these are presented separately. In the Discussion section, we combine information from both sources, pointing out where the observations agree, and where there are inconsistencies. In particular, we find that binding energies calculated from the MD simulations of the protein−ligand interactions, protein−water interactions, and ligand-water interactions agree well with experimental binding enthalpies, suggesting that the models provide a representative picture of the mode of ligand binding and that the compounds bind as anticipated in the design.

MATERIALS AND METHODS

Compound Synthesis. (1*S*)-*endo*-(−)-Borneol *O*-methyl ether was prepared as described by Meerwein and Gerard (1923). The boiling points, refractive indices, and NMR spectra matched the published values. The *O*-allyl and 3,3-dimethyl-*O*-allyl ethers of (−)-borneol were prepared by reacting the potassium salt of (−)-borneol, in dimethyl ethylene glycol, with allyl bromide and dimethyl allyl bromide, respectively. The compounds were purified by flash chromatography (dichloromethane). (1*S*)-*endo*-(−)-Borneol *O*-allyl ether: bp 106−110 °C/15 mmHg, n_{20}^{D} 1.4695; NMR (Perkin Elmer RB24, in deuteriochloroform) 5.8, m, 1H; 5.35, m, 1H; 5.15, 5.0, broad doublet, 1H; 3.95, d, 2H; 3.65, 3.5, broad doublet, 1H; 2.25−1.0, m, 1H; 1.75, s, 3H; 1.65, s, 3H; 0.9, s, 6H; 0.85, s, 3H. (1*S*)-*endo*-(−)-Borneol *O*-(3,3-dimethylallyl)ether: n_{20}^{D} 1.4748; NMR, 5.3, t, 1H; 3.9, d, 2H; 3.65, 3.5, broad doublet, 1H; 2.25−1.0, m, 7H; 1.75, s, 3H; 1.65, s, 3H; 0.9, s, 6H; 0.85, s, 3H. (1*S*)-(−)-Borneol *O*-propyl ether was prepared by hydrogenation of the *O*-allyl compound using 10% palladium charcoal in ethanol and was purified by flash chromatography (dichloromethane); bp 110−115 °C /15 mmHg, n_{20}^{D} 1.4568; NMR, 3.6, 3.5, broad doublet, 1H; 3.35, t, 2H; 2.35−1.1, m, 12H; 0.9, s, 6H; 0.85, s, 3H. Elemental analyses (C, H) for the latter three compounds were within 0.5% of the theoretical values.

The chemical structures of camphor and the three novel camphor analogues studied in detail, methyl borneol ether (CEN), propyl borneol ether (CEP), and allyl borneol ether (CAL), are shown in Figure 2.

Experimental Characterization. Cytochrome P450cam wild type and Y96F were generated and purified as previously described (Gunsalus & Wagner, 1978; Atkins & Sligar, 1988). Samples of purified protein were stored at 193 K with camphor and contained no measurable P420. Substrate-free protein was obtained by passage of the sample through a Sephadex G-25 column previously equilibrated at 277 K with the same buffer used for experiments.

The camphor analogues were diluted in an ethanol−water mixture with less than 3% concentration of ethanol in the final samples. Control experiments for camphor binding showed that the addition of small amounts of ethanol had no measurable effect on its dissociation constant.

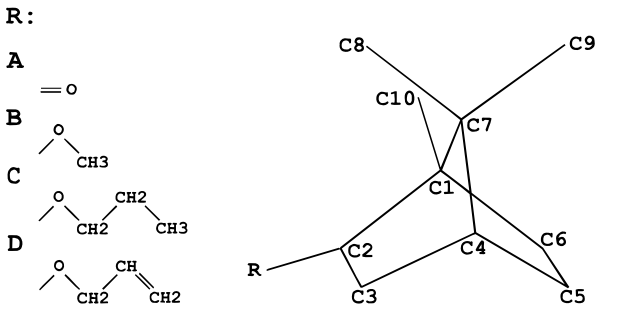

FIGURE 2: Sketches of (A) camphor (CAM), (B) endo-borneol *O*-methyl ether (CEN), (C) *endo*-borneol *O*-propyl ether (CEP), and (D) *endo*-borneol *O*-allyl ether (CAL).

Optical titrations were recorded on a Uvikon spectrophotometer and performed in 100 mM Tris-HCI at pH 7 and 293 K with 2−5 μM cytochrome P450cam. Differential mode at two wavelengths (417 and 392 nm) was used to calculate the overall dissociation constant (K_d) for each ligand by Eadie−Hofstee plots. Thermal regulation of the spectrophotometer was provided by a commercial thermostated circulating bath (Huber HS 40) and allowed the determination of reaction enthalpies over the temperature range of 277−298 K, according to the van't Hoff law.

The high spin content at ligand saturation and 293 K was determined by Christiane Jung's method (Jung *et al.*, 1991).

The spin equilibrium constant (K_{spin} = [P450-high spin]/[P450-low spin]) and the P450 → P420 transition, at saturated ligand concentration, were followed as a function of pressure at 277 K on a Cary 219 spectrophotometer interfaced with a high-pressure bomb. The optical pressure system has been described previously (Hui Bon Hoa *et al*., 1982). The buffer used in pressure experiments was 100 mM Tris-HCl, pH 7/240 mM KCl. The spin reaction volume change $\Delta V_{spin} = V_{HS} - V_{LS}$ and the inactivation reaction volume change $\Delta V_I = V_{P420} - V_{P450}$ were deduced from the relations

$$\Delta V_{spin} = -RT\,(\delta \ln K_{spin}/\delta P)_T$$

and

$$\Delta V_I = -RT(\delta \ln K_I/\delta P)_T$$

respectively.

$$K_I = (a_n - a_p)/(a_p - a_i)$$

where a_p, a_i, and a_n are the absorbances at 404 nm determined in the transition region, in the fully inactivated state, and in the native state, respectively.

Molecular Dynamics Simulations. (1) Parametrization. We used the standard GROMOS force field (van Gunsteren & Berendsen, 1987) within the ARGOS program (Straatsma & McCammon, 1990). United atoms were used for all aliphatic carbons, and only polar hydrogens were modeled explicitly. Water molecules were represented by the SPC/E model (Berendsen *et al*., 1987). Additional parameters for the heme and the camphor analogues are listed in Table 1 and are equivalent to those in our previous work (Helms & Wade, 1995). For the camphor analogues, missing bonded parameters were modeled by analogy to the GROMOS and

Table 1: Force Field Parameters Used in MD Simulations of Complexes of Cytochrome P450cam with Camphor Analogues

(a) Parameters for the Heme with a Cysteine Ligand[a]

	bond parameters	
	r_e (nm)	k (kJ nm^{-2} mol^{-1})
Fe−N	0.209	4.18×10^5
Fe−Sγ	0.220	4.18×10^5

	angle parameters	
	deg	k (kJ rad^{-2} mol^{-1})
Sγ−Fe−N	102	418
Cβ−Sγ−Fe	109.5	251

	LJ parameters	
	A (kJ nm^{-12} mol^{-1})	B (kJ nm^{-6} mol^{-1})
Fe[b]	4.30155×10^{-5}	8.86909×10^{-3}
K[c]	1.06892×10^{-3}	8.89580×10^{-3}

	partial atomic charges q (e)
Fe	1.0
N	−0.4
CH	0.1
CM	0.2
CG	0.27[d]
O1, O2	−0.635[d]

(b) Parameters for Camphor and Camphor Analogues

	proper dihedral force constants[e] (kJ rad^{-2} mol^{-1})		
	CEN	CEP	CAL
C1−C2−O−C11	3.77	3.77	3.77
C2−O−C11−C12		3.77	3.77
O−C11−C12−C13		5.86	5.02 ($\delta = 180°$)[f]

	partial atomic charges q (e)			
	CAM	CEN	CEP	CAL
C2	0.38	0.3	0.3	0.25
O	−0.38	−0.3	−0.45	−0.4
C11		0	0.15	0.15
others	0	0	0	0

[a] Improper dihedrals on pyrrole rings as for histidine, improper dihedrals on propionate groups as for aspartate in the GROMOS87 force field. [b] Taken from Loew (Collins *et al*., 1991). [c] taken from Åqvist (1990). [d] Taken from the aspartate residue of the GROMOS87 force field. [e] All dihedrals have multiplicity $n = 3$. [f] Indicates that the positions of the minima are shifted by 180°.

CHARMM force fields. The barriers for rotation around the side chain torsional angles were determined with MNDO (Dewar & Thiel, 1977), except for the barrier for rotation around the allyl side chain where MNDO gives a rotational profile for the O−CH_2−CH=CH_2 dihedral with 2 instead of 3 minima and the barrier height of ca. 3 kJ/mol is too low. This barrier was calculated with MM3 (Allinger *et al*., 1989), and the results were verified by optimizations of the isolated side chain at 30° intervals with the Gaussian 92 program (1992) at the HF/6-31G* level. The positions of the energy minima for the propyl and allyl side chains are shifted from each other by 60°. Calculations of atomic point charges were performed with the MNDO/ESP method (Besler *et al*., 1990) for the optimized compounds. The calculated partial atomic charges for the united carbon atoms on the "camphor body" were close to 0 (except for the buried C7 atom) and were therefore set to 0. A second set of MNDO/ESP charge calculations was then performed on the isolated side chains with two attached methyl groups in place of C1 and C3. The charges on the side chain atoms were modeled according to the MNDO/ESP results, approximately scaled by 0.6, in order to mimic the typical magnitude of charges in the GROMOS force field.

(2) Setup of Simulations. For dynamic atoms, a twin-range spherical nonbonded cutoff of 0.8 and 1.0 nm was applied. For the atoms in the restrained shell, a 0.8 nm cutoff was used. The solvent−solvent nonbonded pair list was updated every 10 steps, the solvent−solute list every 15 steps, and the solute−solute list every 20 steps. Short-range nonbonded forces were calculated every step, whereas the long-range ones were only updated every fifth step. All bond lengths were constrained with the SHAKE algorithm (Ryckaert *et al*., 1977) with a relative tolerance of 10^{-8}, and a time step of 2 fs was used. During NVT simulations, the solute and solvent parts of the system were separately coupled to a Berendsen thermostat (Berendsen *et al*., 1984) at 300 K with coupling times of 0.1 and 0.4 ps, respectively.

(3) Simulations of the Protein−Ligand Systems. The crystallographic coordinates of cytochrome P450cam, complexed with camphor at 0.163 nm resolution (Poulos *et al*., 1987), were taken from the 2cpp file of the Brookhaven Protein Data Bank (Bernstein *et al*., 1977). The structure consists of residues 10−414 and does not contain coordinates for the first 9 amino acids. An N-terminal blocking group was added to residue 10, and the first 9 residues were omitted for the simulations. The coordinates of the missing atoms of Lys216 were modeled with the QUANTA software package (QUANTA, 1992). Crystallographic water 515 was replaced by a potassium ion because it is octahedrally coordinated by four protein backbone oxygens and two water molecules and specific binding of K^+ to P450cam has been demonstrated experimentally (Di Primo *et al*., 1990). The environment of all Asp, Glu, Arg, Lys, and His residues was analyzed graphically to determine their protonation states. Three histidines were assigned as doubly protonated: His62, His270, and His355. The side chain of Asp297 lies 0.27 nm from one of the heme propionate group oxygens (Poulos *et al*., 1987). To carry out the simulations, either the propionate group or the aspartate side chain must be protonated, although in reality both functional groups could share a common proton. We tried both possibilities in test simulations and found that protonation of Asp297 led to geometries closer to the crystal structure. Hydrogen atoms were added to the polar protein atoms and the 203 crystallographic waters using the ARGOS program (Straatsma & McCammon, 1990). The positions of Tyr, Thr, Ser, and water hydrogens were adjusted by graphical inspection to optimize hydrogen bond formation.

A 3.7 nm sphere of solvent was superimposed on the protein system, the sphere being centered approximately on the geometric center of the active site. All added water molecules closer than 0.26 nm to any non-hydrogen atom of the protein were removed. Four water molecules were put into the active site by the superimposition algorithm. To test whether water molecules should be added in the active site for the simulations, four water molecules were positioned at energetically favorable positions in the active site according to analysis with the GRID program, and a 100 ps simulation was run. In this simulation, there were significant deviations from the crystal structure of the camphor−P450cam complex (the hydrogen bond between camphor and Tyr96 was broken), indicating that the addition of four water molecules was unrealistic. A second test simulation of 200

ps duration was run with one water molecule present at the Fe sixth ligand position (where a water molecule is observed in the crystal structure of the substrate-free enzyme). The average structure calculated from the simulation was similar to that observed experimentally for the camphor−P450cam complex. However, a water molecule is not observed in this position in the crystal structure of camphor complex, and spectroscopic measurements of high-spin content indicate that it is present very rarely. Therefore, further simulations of the camphor and camphor analogue complexes were done without adding water molecules in the active site.

The equilibration of the added solvent shell around the fixed protein was done for the complex of P450cam with camphor. Keeping the water molecules in the outer shell restrained to their positions with a force constant of 2000 kJ nm^{-2} mol^{-1}, the added water molecules within 2.7 nm of the center of the sphere were subjected to 100 steps of steepest descent energy minimization and then equilibrated during 3 successive MD simulations under NVT conditions at 100 K (5 ps), 200 K (5 ps), and 300 K (20 ps).

The heating of the protein was then performed for all camphor analogues separately. After *in vacuo* optimization of the compound geometries with MNDO, they were superimposed onto the position of camphor in the crystal structure, using the aliphatic carbon atoms of the "camphor body" for the structural fit. For CAL and CEP, the compound was turned slightly after superposition to avoid close contacts with the side chains of Phe87 (0.26 nm carbon−carbon distance) and Phe98 (0.30 nm), and then the compound was subjected to 100 steps steepest descent energy minimization with all surrounding atoms fixed. Modeling of the Y96F mutant protein was done by removing the hydroxyl group of Tyr96. All atoms within 1.5 nm of the system center were assigned to be free, and atoms between 1.5 and 1.7 nm were restrained to their crystallographic positions by a weak restraining force of 250 kJ nm^{-2} mol^{-1}. The rest of the system was held fixed, and water molecules beyond 2.8 nm from the center were removed from the system. The system with camphor consisted of 927 dynamic atoms (including 38 water molecules) and 368 atoms in the restrained region. After 100 steps of SD energy minimization, the system was heated with 5 ps of MD at 100, 200, and 300 K under NVE conditions. New atomic velocities were assigned every 0.2 ps according to a Maxwell−Boltzmann distribution. A total of 300 ps of MD simulation was then performed at 300 K under NVT conditions for the wild-type systems and 100 ps of MD for the Y96F mutant systems. Data analysis, including the calculation of nonbonded protein−ligand interaction energies and intraligand side chain energies, was performed on the last 200 ps of the wild type simulations and the last 50 ps of the mutant simulations.

(4) Simulations of the Substrate-Free Protein. The simulations of the substrate-free state were started from the crystal structure (PDB entry 1phc (Poulos *et al.*, 1986)). The setup, the definition of the dynamic region, and equilibration were analogous to the compound simulations. Nonbonded interaction energies between the six water molecules in the active site and the rest of the system were calculated during a 200 ps NVT simulation that followed 100 ps of equilibration. For the simulation of the substrate-free Y96F mutant, six water molecules were assigned in the active site as for wild type. An additional test simulation of the wild-type protein was run for 100 ps with eight waters in the active site as a test of sensitivity to the extent of hydration of the active site. The eight water molecules stayed in the active site during the simulation.

(5) Simulations of the Compounds in Aqueous Solution. Structures of the compounds that had been optimized *in vacuo* (see above) were solvated in cubic boxes of SPC/E water with 2.4 nm long edges. The aqueous system with camphor contained 448 water molecules. A total of 200 ps of MD equilibration was performed under NPT conditions at 300 K, followed by another 200 ps of analysis in which the nonbonded energies between the compound and the solvent, and the intraligand side chain energies, were calculated (coordinate sets were stored every 0.1 ps). The solvent distribution around the compounds was analyzed, and the number of solvent molecules within the first hydration shell layer was calculated.

(6) Calculation of Errors in Energies from Simulations. Errors are given as $\sigma/n^{1/2}$, where σ is the standard deviation and n is the number of data points. The data points can be considered as uncorrelated because they are separated by at least 50 MD steps. By analyzing the data in four separate time intervals, we ensured that there is no drift in the mean interaction energy. The standard error of the protein−ligand interaction energy is typically 0.4 kJ/mol for the 200 ps of data acquisition for wild-type simulations and 0.7 kJ/mol for the 50 ps of data acquisition in the Y96F simulations. The standard error for the simulation of the six water molecules in the P450cam active site is 0.5 kJ/mol. The standard error for six water molecules in bulk solvent is very small (0.05 kJ/mol), because all 460 solvent molecules were used for the calculation of the interaction enthalpy. For the cycle (3 + 4) − (1 + 2) (see Results section), the errors in all legs of the cycle are simply summed. The summed errors are between 1.2 and 1.8 kJ/mol. Further, we calculated the standard errors of the intraligand side-chain contributions in the same way. The summed contributions from the simulations in protein and in aqueous solution are between 0.3 and 0.7 kJ/mol. The simulation errors are therefore between 1.6 and 2.5 kJ/mol.

(7) General Properties of the Camphor Analogues. Solvent-accessible surface areas were calculated with the GRASP program (Nicholls & Honig, 1991) by rolling a 0.14 nm radius probe over the molecular surface. The dipole moments and the aqueous solvation free energies were calculated by the semiempirical AM1-SM2 method (Cramer & Truhlar, 1992) with the AMSOL5.0 program (Cramer *et al.*, 1995).

RESULTS

Experimental Results. Figure 3 displays the high spin content of the Fe atom in the P450cam−ligand complexes in the presence and absence of 200 mM KCl. The values for CAM (98% high spin for wild type and 54% high spin for Y96F, in the presence of K^+) are in accordance with previous work (Atkins & Sligar, 1988; Di Primo *et al.*, 1990). For wild-type P450cam, CAL has a similar high spin content to CAM and the values for CEN and CEP are slightly lower than for CAM. For Y96F, the high spin content is almost the same as for wild type for CEN and is higher than for wild type for CEP and CAL. This is in clear contrast to CAM, which shows a large spin decrease for Y96F compared

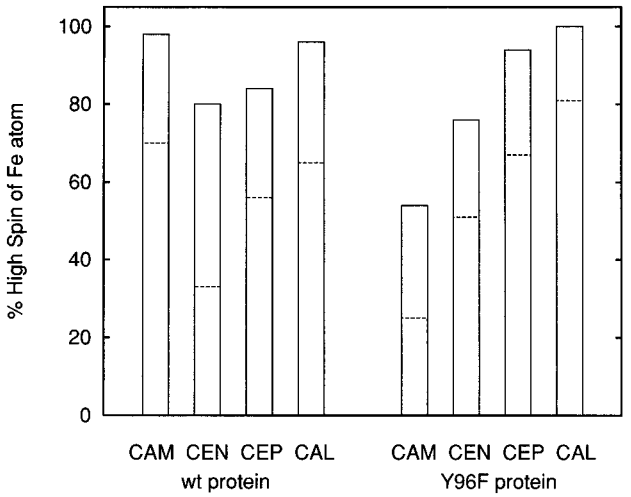

FIGURE 3: Experimental Fe high spin content for wild-type and Y96F cytochrome P450cam with camphor CAM and its analogues CEN, CEP, and CAL bound. The solid boxes show the results in the presence of 200 mM KCl, and the dashed lines give the results without KCl.

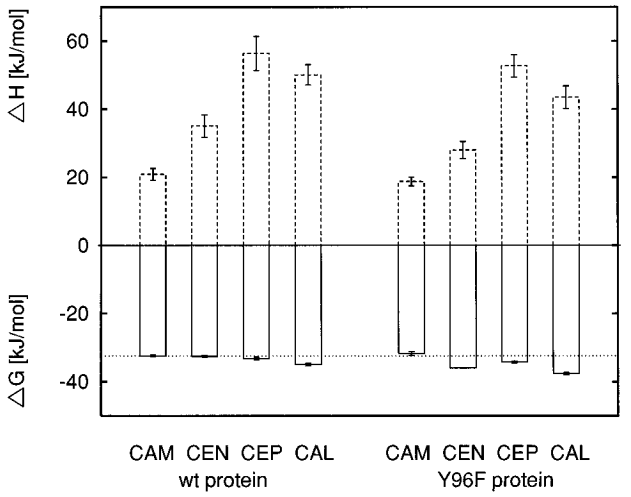

FIGURE 4: Experimental binding enthalpies (dashed lines) and binding free energies (solid lines) with error bars for the binding of camphor (CAM) and its analogues CEN, CEP, and CAL to wild-type and Y96F cytochrome P450cam. The dotted line marks the binding free energy of camphor to wild-type P450cam.

to wild type. Compared to the data in the presence of K^+, the high spin content is lower in the absence of K^+ for all compounds. For wild type, the decrease is moderate for CAM, CEP, and CAL (ca. 30%) and more pronounced for CEN (47%). For Y96F, the high spin content decrease is similar for all compounds (ca. 20−30%) but results in CAM having a high spin content of only 25%.

Figure 4 shows ligand binding enthalpies and binding free energies for wild type and Y96F. For wild type, the binding free energy for CEN is identical to that for CAM, and the binding free energies for CEP and CAL are more favorable than for CAM by 0.4 and 2.5 kJ mol^{-1}. For Y96F, the binding free energy of CAM is less favorable than for wild type by 0.8 kJ mol^{-1}, whereas the binding free energies for CEN, CEP, and CAL are more favorable than for wild type by 3.3, 1.3, and 2.5 kJ mol^{-1}. As noted before for camphor and other compounds (Fisher & Sligar, 1985, 1987), K_d and K_{spin} (spin equilibrium constant) are independent quantities and do not show identical trends. As the size of the compound increases (CAM−CEN−CAL−CEP), the binding

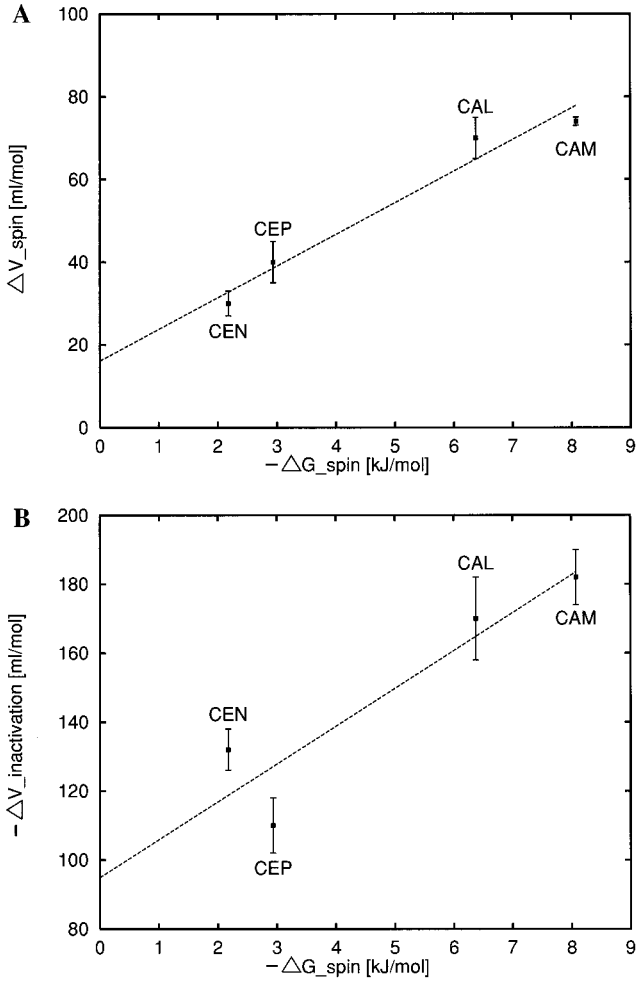

FIGURE 5: Experimental volume changes for the protein−ligand complexes upon application of hydrostatic pressure. (A) The spin reaction volume change is plotted against the spin free energy change. (B) The negative of the inactivation reaction volume is plotted against the spin free energy change.

enthalpies become more unfavorable and the binding entropies become more favorable for both wild type and Y96F. The binding enthalpies and entropies of all compounds are less positive for Y96F than for wild type.

The changes in spin reaction volume, ΔV_{spin}, following the spin conversion from high spin to low spin under the application of high pressure and the changes in inactivation reaction volume, $\Delta V_{inactivation}$, following the interconversion of P450cam to the inactive form P420 have been measured for CAM, CEN, CAL, and CEP. Figure 5A shows the spin reaction volume changes plotted against ΔG_{spin}, and Figure 5B shows the inactivation reaction volumes. Both types of volume change are linearly related to ΔG_{spin}, and the same trends are observed for the series of compounds.

Simulation Results. The protein dynamics are very similar for all of the compounds with respect to the RMS deviation from the crystal structure, RMS atomic fluctuations, hydrogen bond patterns, and the RMS fluctuation of the torsional angles. For wild type, the RMS deviation of the average simulation structure from the initial camphor crystal structure is 0.051 nm for CAM and CAL, 0.055 nm for CEN, and 0.056 nm for CEP (non-hydrogen atoms of protein and ligand). The RMS deviations between the average simulation structures with different ligands are between 0.014 nm (CAL−CEP) and 0.018 nm (CAL−CAM). The results for

Y96F (from shorter simulations) are in the same ranges. The RMS atomic fluctuations of the active site residues are in the range between 0.035 and 0.050 nm and do not show significant differences between MD simulations of the various compounds and between simulations of the wild type and Y96F protein. The RMS fluctuations of the backbone dihedrals in the dynamic region have a range of 17.4−17.6° for Φ and 16.0−16.9° for Ψ in the simulations for wild type. The values for Y96F are higher (22.4° for Φ and 19.7−20.7° for Ψ), but they agree well with values calculated from the corresponding part of the wild-type trajectory. The side chains of the novel camphor analogues were initially modeled into the hydrophobic cavity close to site D. These modeled starting configurations were stable during the MD simulations, and the side chains made favorable van der Waals interactions with the surrounding hydrophobic protein residues. The ligand conformations sampled in the MD simulations for the Y96F protein mutant were very close to those in the simulations for wild-type protein, except for camphor which turned around in the active site and formed a weak hydrogen bond with Thr101 which lost its native hydrogen bond with Tyr96. Panels A, B, C, and D of Figure 6 show average structures of CAM, CEN, CEP, and CAL and the active site residues during the MD simulations of wild type. Figure 6E shows the unusual average conformation of camphor during the simulation of Y96F. Table 2 lists average distances between the ligands' side chain oxygen and the Tyr96 hydroxyl oxygen. For camphor, the distance corresponds to the length of an optimal hydrogen bond with low length fluctuation. The distance for CEN is slightly longer but shows low fluctuations as well. For CEP and CAL, the distance is 0.31 nm with a larger fluctuation of 0.04 nm. The distances to Phe96 are longer by 0.24 nm on average, but 0.06 nm of this difference is due to the fact that the distances are calculated to the CZ of Phe96 instead of the OH of Tyr96. CEP lies closest to Phe96, whereas the distance of CEN to Phe96 fluctuates the most. It is unclear from MD simulations of this length whether the ligand side chains are conformationally more restricted in the protein than in solution because the number of dihedral transitions is quite small (the most floppy dihedral, O−C11−C12−C13, only makes 11 transitions during the simulation of CAL in aqueous solution, and 8 in the case of CEP). For CAL, the number of dihedral transitions is similar in protein and solution, whereas for CEP it is smaller in the protein simulation. The number of sampled dihedral minima is the same for CAL, but it is smaller for CEP in the protein. We find a slightly higher flexibility for the CAL side chain, compared to the CEP side chain.

In order to compare a property derived from the simulations with the experimental Fe high spin content, we calculated the distances between all ligand atoms and the Fe atom. A crowding of close ligand atoms around the Fe atom could indicate better shielding of the Fe atom from solvent. Ligand atoms at distances less than 0.5 nm are considered as "close" atoms because at such a distance a water molecule cannot fit directly between the ligand atom and the Fe atom. Table 3 lists the names of all close atoms for wild type and Y96F. Three carbon atoms of CAM are close atoms for wild type, but only two for Y96F. CEN, CEP, and CAL have one close atom for wild type and two close atoms for Y96F.

Non-bonded interaction energies were calculated between each ligand and the rest of the system, including protein and solvent molecules. The LJ energies (Figure 7A) for the simulations in aqueous solution are much more favorable than for the protein simulations due to better packing of the water molecules around the solute molecules. The bigger the compounds are, the more favorable are the LJ energies, in both the protein simulations and those in aqueous solution. With the exception of camphor, the interaction energy with the Y96F mutant is less favorable than for wild type.

The electrostatic energies (Figure 7B) are more favorable in aqueous solution than in the protein as well. This is so even though the dielectric constant of water is much higher than that of protein. It results from the presence of a large number of polar groups in the bulk phase (surrounding water molecules) in close vicinity to the compounds, whereas most protein side chains in the protein active site are hydrophobic and have zero or low atomic charges assigned. Therefore, the electrostatic contribution is mostly due to close water molecules. The difference in the water and protein dielectric constants is more important for long-range electrostatic effects. In the case of the camphor ligands, long-range electrostatic effects are expected to be small because these ligands are quite nonpolar.

The left side of Figure 8 displays how the difference in enthalpy for unbound and bound protein is measured by experiment. In order to calculate enthalpies by MD simulation that are comparable to the experimental results, the difference (3 + 4) − (1 + 2) needs to be calculated (right side of Figure 8). If only (4 − 1) is calculated, i.e., the difference between the nonbonded energies of the ligand in the protein (4) and in aqueous solution (1), the wild-type energies are more favorable than the Y96F energies, which is not in agreement with experiment. To account for parts (2) and (3), simulations were performed of the unbound protein with the active site filled by six water molecules as in the crystal structure and of the six water molecules in bulk water. For simplicity, we assumed that the active site of Y96F P450cam is also filled by six water molecules, although this might not be the case. The water binding enthalpies were −242.6 kJ mol^{-1} for the six water molecules in the wild-type active site and −228.4 kJ mol^{-1} for Y96F. The average enthalpy of six SPC/E waters in bulk SPC/E water was calculated as −274.6 kJ mol^{-1} from a 300 ps simulation of 460 SPC/E water molecules. The release of the six active site water molecules to the solvent (3 − 2) is therefore enthalpically favorable for both wild type and Y96F mutant, but it is more favorable for wild type by −14.2 kJ mol^{-1}. Intraprotein and protein−solvent energetic contributions to the binding of different ligands and the intraligand energetic contributions of the camphor body were neglected. However, the intramolecular energy contributions of the ligands' side chains were calculated. The difference between the side-chain intramolecular energy in the simulations in protein and in aqueous solution is generally less than 2 kJ/mol, except when CAL and CEP are compared in wild-type protein and in aqueous solution when the difference is 5.2 and 6.2 kJ/mol, respectively. This results from slightly strained side-chain conformations of CAL and CEP with higher angle and dihedral energies in order to maximize the strength of the hydrogen bond to Tyr96 in the native protein. Binding to the native protein by CAL and CEP is therefore slightly unfavored with respect to the

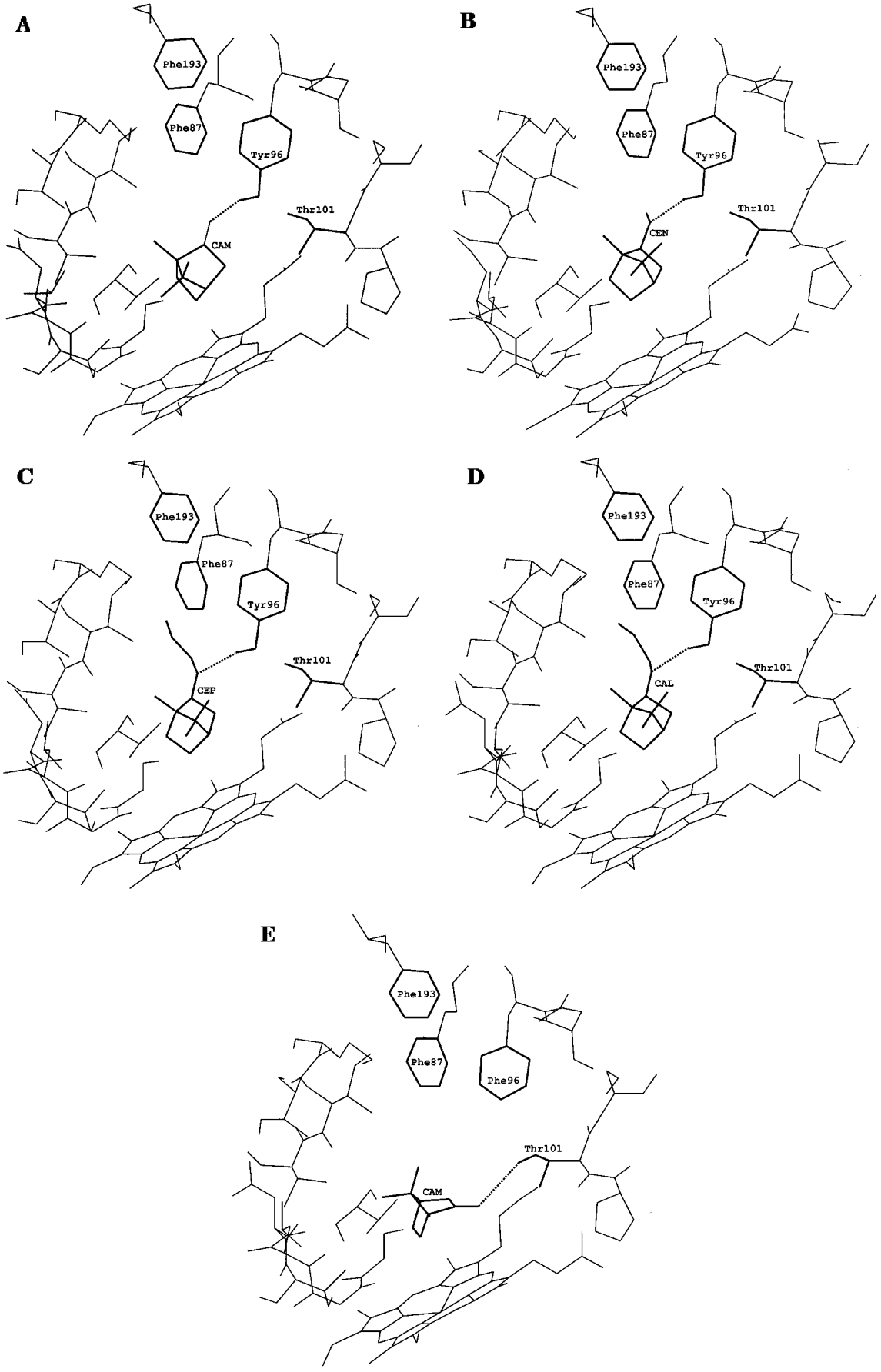

FIGURE 6: Average structures of the ligand and the surrounding active site residues from MD simulations of wild-type cytochrome P450cam with (A) camphor, (B) CEN, (C) CEP, and (D) CAL. (E) shows the average structure of camphor when simulated in the P450cam mutant Y96F. The dashed lines indicate hydrogen bonds with Tyr96 or Thr101 (E).

Table 2: Average Distances (nm) from Y96:O and F96:CZ to the Ligand Side-Chain Oxygen during the MD Simulations

	CAM	CEN	CEP	CAL
wild type	0.28 ± 0.02[a]	0.30 ± 0.02	0.31 ± 0.04	0.31 ± 0.04
Y96F	0.55 ± 0.07	0.57 ± 0.06	0.49 ± 0.04	0.55 ± 0.04

[a] Standard deviation.

Table 3: Ligand Atoms within 0.5 nm of the Fe Atom during MD Simulations of Cytochrome P450cam with Camphor and the Camphor Analogues

	CAM	CEN	CEP	CAL
"close atoms" wild type	C4, C5, C9	C5	C5	C5
"close atoms" Y96F	C5, C6	C5, C9	C5, C9	C5, C9

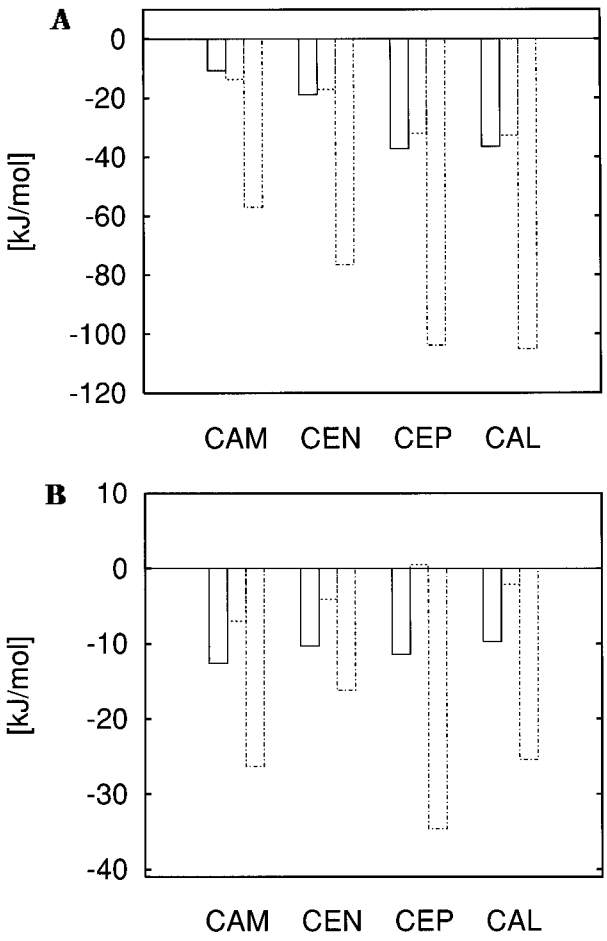

FIGURE 7: Calculated nonbonded Lennard-Jones energies (A) and nonbonded electrostatic energies (B) from the MD simulations of the four different ligands. For each ligand, three values are given which represent the average value during the simulations with wild-type P450cam (—), with Y96F P450cam (- - -), and in aqueous solution (-•-).

ligands' internal energy compared to binding to Y96F. The calculated energies reproduce the experimental trends (see Figure 9), and the largest deviation is 9 kJ mol^{-1} for CEP in Y96F.

Table 4 contains physicochemical properties of the ligands: the solvent-accessible surface area (SASA), the relative difference in SASA compared to camphor, the number of solvent molecules in the first hydration shell in the simulations of the compounds in aqueous solution, the average SASA of the solute per solvent molecule in the first hydration shell, the relative difference in the number of

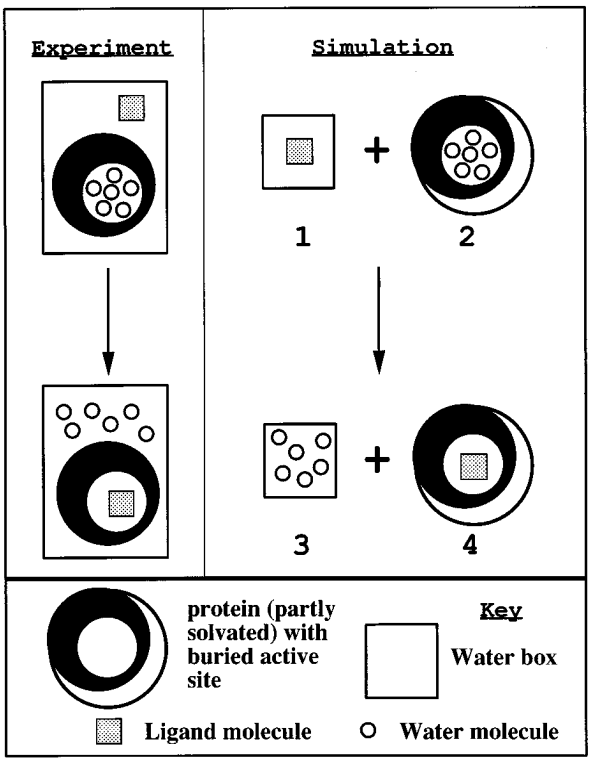

FIGURE 8: Schematic representation of the binding of a ligand to cytochrome P450cam in an experiment (left side) and a simulation (right side). The symbols used are explained in the key. Ligand binding is modeled as inducing the release of six water molecules from the active site. The simulation part shows four systems (see text) that all need to be simulated in order to yield results comparable to experimental values.

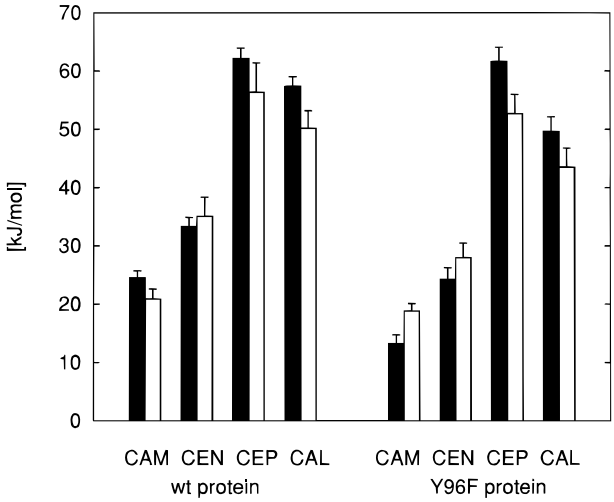

FIGURE 9: Comparison of the calculated binding enthalpies from MD simulations (black boxes) and the experimental binding enthalpies (empty boxes) for the binding of camphor (CAM) and the camphor analogues CEN, CEP, and CAL to wild-type and Y96F mutant P450cams.

hydration waters compared to camphor, the dipole moments, and the calculated hydration free energies of the compounds. The size of the compounds increases in the series CAM−CEN−CAL−CEP. The number of close water molecules in the first hydration shell is, to within a good approximation, proportional to the solvent-accessible surface area of the compounds. An average solvent-accessible surface area per water molecule of ca. 0.105 nm^2 was calculated. The average SASA of the solute per solvent molecule in the first hydration shell is a little higher for camphor than for the other

Table 4: Physicochemical Properties of Camphor and the Camphor Analogues

	CAM	CEN	CEP	CAL
SASA (nm^2)[a]	3.22	3.43	4.08	3.94
ΔSASA (nm^2)[b]		0.21	0.86	0.72
#wat: number of solvent molecules in hydration shell[c]	28.4	33.2	39.4	39.2
SASA per solvent molecule in hydration shell (nm^2)[d]	0.113	0.103	0.104	0.101
Δ#wat[e]		4.8	11.0	10.8
dipole moment (D)[f]	4.0	1.4	1.3	1.4
ΔG_{hydr} (kJ mol^{-1})[f]	−13.8	7.1	11.3	9.4

[a] Calculated with the GRASP program (Nicholls & Honig, 1991) for a 0.14 nm radius probe. [b] ΔSASA(compound) = SASA(compound) − SASA(camphor). [c] From MD simulation of the compounds in aqueous solution. [d] SASA per solvent molecule in hydration shell = SASA/#wat. [e] Δ#wat(compound) = #wat(compound) − #wat(camphor). [f] Calculated with the AM1-SM2 Hamiltonian in the AMSOL 5.0 program (Cramer *et al.*, 1995).

compounds. The dipole moments of the new camphor analogues are lower than that of camphor, and this is a factor contributing to the less favorable solvation free energies for CEN, CEP, and CAL in aqueous solution than for CAM.

Table 5 lists the experimental binding entropies and the relative differences in binding entropy of the camphor analogues compared to camphor. The ratios of the relative entropy difference to the relative difference in SASA and to the relative difference in the number of hydration waters are listed. The ratios for CEP and CAL are very similar, and the ratios for CEN are a bit higher. The ratios for all compounds are similar for wild type and Y96F.

DISCUSSION

The natural substrate of cytochrome P450cam, camphor, is oriented in the active site of P450cam by one specific hydrogen bond with Tyr96 and by complementary hydrophobic contacts. But enough space is left free in the active site to accommodate a number of water molecules, in particular in a hydrophobic part of the active site close to Tyr96, Phe87, and Phe193. Wade (1990) expected improved binding for a camphor analogue with a hydrophobic moiety that could point into this region, making better van der Waals contacts with the surrounding residues and excluding solvent from this region. In this work, four novel camphor analogues have been synthesized and their binding to P450cam has been characterized by experimental and simulation techniques. The following discussion first addresses the binding affinity of the compounds, and an explanation of the experimental observations is provided. Then, we consider the binding enthalpy, the binding entropy, and the Fe high spin content of the compounds individually. Finally, we draw conclusions.

Binding Free Energy. The novel camphor analogues bind equally well (CEN) or better (CEP, CAL) to wild type than camphor. Further extension of the hydrocarbon chain was tested by the synthesis of a dimethylallyl *O*-borneol ether compound, but the experimental binding free energy was less favorable (K_d = 8.4 μM) than for CAM, CEN, CEP, and CAL. Modeling of the dimethylallyl compound into the region near site D in the crystal structure by an analogous procedure to that for the other fragments showed that the dimethylallyl side chain cannot be modeled pointing in the direction of site D without making sterically conflicting contacts to neighboring residues. This indicates that, in order to allow binding of the dimethylallyl compound, the protein structure has to open up somewhat. Thus, as predicted from the modeling, a 3-carbon chain substituent is the optimum length for optimum binding affinity.

The gain in binding affinity is, however, modest. It is consistent with that found for the binding of ligands with hydrocarbon chains of differing length to carbonic anhydrase (Gao *et al.*, 1995). The change in binding free energy for different series of compounds correlated reasonably well with the change in molecular surface area with $\Delta G/\Delta A = -2.9$ to -11.3 kJ nm^{-2} mol^{-1}. In our case, the difference in molecular surface area (not solvent accessible surface area) between camphor and the best binding compound CAL is ca. 0.45 nm^2. One would therefore expect an improvement by ca. −1.3 kJ/mol to −5.1 kJ/mol. The measured value of −2.5 kJ/mol fits into this range well. Other studies show, however, that the addition of a methyl group can result in binding affinity changes outside this range. An example where it is enhanced is given by Verlinde *et al.* (1994), who describe a methyl substitution that improves the binding of adenosine to GAPDH 8−12.5-fold. Vermersch *et al.* (1991) studied complexes of arabinose-binding protein with arabinose (Ara) and fucose (Fuc) where the equatorial H of Ara in the C5-position is substituted for CH_3. For wild type, the affinity is higher for Ara than for Fuc (K_d = 0.1 μM vs 3.8 μM), whereas for a M108L mutant, the trend is inversed (K_d = 0.44 μM for Ara vs 0.35 μM for Fuc). In these two examples, the change in binding affinity depends on whether the steric fit between ligand and protein is improved or worsened. However, in the first case, it is apparent that the large increase in binding is also dependent on other factors, e.g., the displacement of an ordered water molecule or a significant difference in binding mode. In general, the addition of a hydrocarbon moiety to a ligand should enhance binding unless it results in steric conflict. However, big improvements in binding may only result from the optimization of other factors alongside steric complementarity.

In contrast to camphor, the novel camphor analogues bind more strongly to Y96F than to wild type (K_d = 0.2 ± 0.02 μM for CAL), and this may at first seem surprising in view of the loss of the hydrogen bond to Tyr96. However, mutation of a residue that can make a hydrogen bond to a ligand into a residue that cannot does not usually alter the net hydrogen bond balance on ligand binding because a water molecule can often make a hydrogen bond to the unliganded wild type residue (Fersht *et al.*, 1985). On the other hand, the displacement of the water molecule by the ligand on binding the wild-type protein will make a favorable binding entropy contribution (Fersht *et al.*, 1985). An illustrative example of the effect of mutating Tyr into Phe on ligand binding is a study of the binding of FK506 to FKBP-12 protein by microcalorimetry and crystallography (Connelly *et al.*, 1994). The mutation abolishes a protein−ligand hydrogen bond and leads to a reduced binding affinity although binding to the mutant is accompanied by a more favorable enthalpy change. In unliganded wild-type FKBP-12, two water molecules form hydrogen bonds with the tyrosine, and they are displaced upon formation of the protein−ligand complex. No water molecules are found close to Phe in the mutant. Therefore, the overall entropic advantage of displacing two water molecules upon binding leads to a slightly more favorable binding free energy for

Table 5: Interpretation of ΔS_{exp} as Desolvation Entropies

	binding to wild type				binding to Y96F			
	CAM	CEN	CEP	CAL	CAM	CEN	CEP	CAL
ΔS_{exp} (J K^{-1} mol^{-1})	182.7 ± 12.3	231.2 ± 14.4	305.1 ± 16.5	290.9 ± 17.9	172.6 ± 10.8	218.2 ± 11.3	296.8 ± 15.1	276.7 ± 12.2
$\Delta\Delta S$ (J K^{-1} mol^{-1})[a]		48.5 ± 26.7	122.4 ± 28.8	108.2 ± 30.2		45.6 ± 22.1	124.2 ± 25.9	104.1 ± 23.0
$\Delta\Delta S/\Delta$#wat (J K^{-1} mol^{-1})[b]		10.1	11.1	10.0		9.5	11.3	9.6
$\Delta\Delta S/\Delta$SASA (J K^{-1} nm^{-2} mol^{-1})[c]		231.0	142.3	150.3		217.1	144.4	144.6

[a] $\Delta\Delta S$(compound) = ΔS_{exp}(compound) − ΔS_{exp}(camphor). [b] Δ#wat is the difference of the number of solvent molecules in the hydration shell of the compound compared to camphor; compare Table 4. [c] ΔSASA is the difference in solvent-accessible surface area compared to camphor; compare Table 4.

wild type. A recent MD simulation for this system reproduced the experimental free energy and confirmed that the release of the two water molecules favors binding to the wild-type protein (Pearlman & Connelly, 1995). A similar argument could apply to cytochrome P450cam. Although none of the water molecules in the substrate-free crystal structure are within hydrogen bonding distance of Tyr96, we always observed one water molecule making a hydrogen bond to Tyr96 in the MD simulation of the substrate-free wild-type protein. This would indicate an entropically slightly more favorable binding to wild type. On the other hand, compounds which do not form a hydrogen bond with Tyr96 at all, or only make a weak hydrogen bond, are expected to bind better to Y96F than to wild type for enthalpic reasons. The experimental data suggest that this is the case for CEN, CEP, and CAL. The same conclusion can be drawn from the MD simulations, where the hydrogen bond lengths for CEP and CAL are equal to or greater than 0.30 nm and show large fluctuations, whereas the camphor hydrogen bond has an optimal length of 0.28 nm. For CEN, the effect is not so pronounced. These observations on hydrogen bond formation agree with statistical analysis of small molecule crystallographic data (Murray-Rust & Glusker, 1984) that indicates that ether oxygens with sp^3 hybridization form weaker hydrogen bonds than carbonyl oxygens with sp^2 hybridization.

We did not attempt to calculate relative binding free energies for the camphor analogues because only a few conformational transitions were observed during the MD simulations of the camphor analogues. The standard molecular dynamics method may not be adequate for studying the accessible conformational space in the P450cam active site of the relatively large compounds studied here (in comparison to camphor), and more sophisticated ways of sampling the conformational space may need to be employed.

However, an important contribution to the improved binding of the novel camphor analogues comes from their increased hydrophobic character compared to camphor, and we have therefore calculated solvation free energies with the AM1-SM2 method. Although the AM1-SM2 method was parametrized to reproduce experimental data for smaller organic molecules, the calculated value for camphor of −13.8 kJ mol^{-1} is very close to the experimental value of −14.8 kJ mol^{-1} (derived from the vapor pressure (Datin, 1916) and the solubility in water (Ishizaka, 1914)). No experimental data are available for the other compounds. The AM1-SM2 hydration free energies for the novel analogues are unfavorable relative to camphor by 20.9 kJ mol^{-1} (CEN), 24.9 kJ mol^{-1} (CEP), and 23.2 kJ mol^{-1} (CAL). This trend is to be expected due to the lower dipole moment of the camphor analogues.

Thermodynamic analysis shows that the binding of the small ligands CAM, CEN, CEP, and CAL to P450cam is characterized by enthalpy−entropy compensation. With increasing compound size, both enthalpy and entropy become more positive, so that overall the binding free energy is only slightly more favorable. These two contributions are analyzed separately in the following two sections.

Binding Enthalpies. The experimentally observed binding enthalpies of all four compounds in both wild type and Y96F are very well reproduced by the calculated enthalpies. The simulation results also agree with experiment in predicting less positive binding enthalpies for Y96F than for wild-type protein. In our computation of enthalpies from the simulations, we only include nonbonded interaction energies between the protein and the ligand, and intraligand side-chain energies, since it is known that the total system enthalpy including intraprotein interactions is subject to large fluctuations over long time scales (Kollman, 1993). In the case of P450cam, the neglect of the intraprotein interactions is supported by the similarity of (a) the crystal structures of P450cam with a number of ligands and the ligand-free structure (Poulos *et al.*, 1986, 1987; Poulos & Howard, 1987; Raag & Poulos, 1989, 1991) and (b) the protein structure in the average MD coordinates of complexes with different ligands. The close agreement of calculated and experimental enthalpies and the correct reproduction of various trends for different ligands show the method to be a useful tool for the analysis of MD simulations of protein−ligand complexes. Nevertheless, the method is only suitable for systems where the protein conformational changes are minimal when a ligand is bound. Further, it is essential to include all necessary solvent contributions (see Figure 8). We are not aware of previous simulations, in which solvent contributions have been included in this way. The release of the active site water molecules is enthalpically favorable, and only the inclusion of this solvent contribution can reproduce the experimental observation that the enthalpies for Y96F are more favorable than for wild type. Unrealistic treatment of solvent such as in the test simulation for the camphor−P450cam complex when four water molecules were placed in the active site can lead to binding enthalpies inconsistent with experiment (ca.15 kJ/mol too large for camphor binding to wild-type P450cam). However, binding enthalpies calculated for camphor binding to wild-type P450cam are insensitive to whether a water molecule is included at the sixth ligand position in the complex or not, and whether the substrate-free enzyme active site contains six or eight water molecules.

Binding Entropies. The experimental binding entropies are all positive and increase with increasing compound size. The ratios of binding entropies to solvent-accessible surfaces

are between 56.7 J mol^{-1} K^{-1} nm^{-2} for camphor and 74.8 J mol^{-1} K^{-1} nm^{-2} for CEP. For comparison, the corresponding number for the transfer of hexane from water to its own liquid is 38.4 J mol^{-1} K^{-1} nm^{-2} (calculated from the experimental transfer entropy of 109.1 J mol^{-1} K^{-1} (Baldwin, 1986) and the SASA of hexane of 2.84 nm^2). This indicates that the binding entropy can be partly, but not fully, accounted for by desolvation of the ligands. Binding entropies may be considered to be due to distinct contributions (see, e.g., Murphy *et al.*, 1995). We calculated differences in the binding entropies of the compounds relative to camphor and compared them to relative differences in surface area and the number of water molecules in the hydration shell (see Table 5). Assuming similar binding modes for the ligands, the relative entropies ($\Delta\Delta S$) can be expected to be independent of the entropic contributions due to the loss of configurational entropy of the protein side chains, the loss of entropy of the ligand due to the decrease in its translational and rotational degrees of freedom, and the gain in entropy due to the release of solvent from the active site. Any contribution due to the relative side chain torsional entropy of CAL and CEP can be expected to be small because their side chains show similar mobility in simulations in the protein and in solution. In support of this idea, the ratios of the relative binding entropies of the analogues ($\Delta\Delta S$) to the relative number of hydration water molecules (Δ#wat) are very similar for all compounds and suggest an entropic desolvation contribution of ca. 10 J mol^{-1} K^{-1} per water molecule. But, although the number of water molecules in the first hydration shell correlates well with the solvent-accessible surface area, the analogous values for the ratio of the relative binding entropy to the difference in SASA are more spread because ratios of small differences are compared. The approximate average value of this ratio of 200 J mol^{-1} K^{-1} nm^{-2} is much greater than the experimental value for the transfer of nonpolar solutes from aqueous to hydrophobic solvent as given above. One reason is that camphor is more polar than the camphor analogues as indicated by its larger dipole moment, and therefore, the calculation of properties relative to camphor will not give comparable results to those from a series of hydrocarbons. But the deviation also indicates that the analysis above is oversimplified and other contributions to the binding entropy should not be neglected, e.g., the decrease in torsional flexibility of the ligands upon binding.

High Spin Content. Our interpretation of the experimental high spin results will follow that of previous work: The percentage of high spin reflects the solvent accessibility of the Fe atom (Fisher & Sligar, 1985), which itself is related to the mobility of the ligand in the active site. K^+ binds in an octahedral coordination provided by the carbonyl backbones of Tyr96, Gly93, Glu94, Glu84, and waters 517 and 584 (Poulos *et al.*, 1987) and therefore has a local rigidifying structural effect by stabilizing the Tyr96 backbone (Di Primo *et al.*, 1990). For wild-type cytochrome P450cam, the heme region is more accessible to solvent for CEN and CEP than for CAM and CAL. For Y96F, CEP and CAL exclude almost all solvent from the heme region, indicating low mobility and good fit of the ligands. CAM on the other hand is much more mobile for Y96F. In the absence of K^+, the results are similar for all compounds: Fe is more accessible to solvent, which can be explained by a looser active site framework and higher mobility of the compounds.

The structural effect of potassium binding could not be addressed in the MD simulations because the potassium binding site was close to the fixed atom region in our system setup. Table 3 lists the ligand atoms that are closer than 0.5 nm to Fe and therefore shield the Fe atom from any solvent. CAM has 3 close atoms for wild type, but the close atom C9 is lost for Y96F. This could reflect the sharp decrease in high spin content for Y96F. CEN, CEP, and CAL have only one close atom for wild type, but two close atoms for Y96F. This parallels the similar (CEN) or higher spin content for the mutant (CEP and CAL). This interpretation should, however, be considered preliminary since it is unclear whether sufficient ligand conformations are sampled in the simulations, and simulations for all compounds with solvent molecules included in the active site might give different results. In particular, experimental evidence suggests that camphor is more mobile in the active site of Y96F than in wild type and the unanticipated conformations observed in the MD simulations might only be a minor subset of those populated. We note that this analysis does not explain why CAL and CEP have such high spin content for wild type compared to CAM.

We now discuss the relation between the Fe high spin content data and the formation of a hydrogen bond with Tyr96. For wild type P450, camphor forms a strong hydrogen bond that restricts its motion. The sharp decrease in high spin content for the camphor−Y96F complex can be explained by the higher mobility of camphor in the active site because it is not stabilized by the Tyr96 hydrogen bond. CEN has a lower high spin content than the other compounds in wild-type P450 and seems only to form a weak hydrogen bond to Tyr96. Surprising are the greater high spin contents for CAL and CEP in Y96F than wild type, which indicates that formation of the Tyr96 hydrogen bond is not important for the stabilization of these ligands in the active site.

Application of hydrostatic pressure shows that the wild-type protein active site is least likely to be hydrated when CAM and CAL are bound, whereas CEN and CEP may allow for some active site solvation. This interpretation is also in agreement with the lower high spin content of CEN and CEP for wild type than camphor. The linear relationship for $\Delta V_{inactivation}$ was previously found for a series of commercially available ligands (Di Primo *et al.*, 1992), but the linear relationship for ΔV_{spin} has not been reported so far. We will address the use of hydrostatic pressure for studying the solvation of the active site in more detail in a subsequent paper.

Conclusions. The camphor analogues with a 3-carbon substituent have very high Fe spin ratios and K_d values for binding that are consistent with our prediction. The improved binding compared to camphor results primarily from the greater hydrophobicity of the compounds and the consequently less favorable free energy of solvation. However, their complementarity to the shape of the protein binding site is important, and compounds with a 3-carbon substituent bind better than those with smaller or larger substituents. The camphor analogues bind better to the Y96F mutant protein because they do not form strong hydrogen bonds with Tyr96 in wild-type P450cam. The MD simulations show that the modeled compound orientations are at stable local energy minima although other binding modes that were not sampled during the simulations may be possible. As compound size increases, binding enthalpy and

entropy increase with almost perfect compensation. The simulations can reproduce the experimental binding enthalpies well and provide a reasonable interpretation of the experimental Fe high spin content and the experimental binding entropies. In conclusion, binding affinity can be improved by adding a nonpolar moiety to the ligand of appropriate size to fill extra space in the binding pocket that is not occupied by ordered water but enthalpy−entropy compensation means that changes in the free energy of binding are likely to be small.

ACKNOWLEDGMENT

We thank T. P. Straatsma for the provision of the ARGOS program, S. G. Sligar for kindly providing us with the fermentation facilities of his laboratory, and C. Di Primo for preparing the Y96F protein, N. Allinger for the provision of previously unpublished MM3 parameters for the allyl compound, and P. Goodford, B. Steipe, and V. Lounnas for critical comments on the manuscript. Access to computing facilities at the Höchstleistungsrechenzentrum (HLRZ) in Jülich is gratefully acknowledged.

REFERENCES

Allinger, N. L., Yuh, Y. H., & Lii, J. H. (1989) *J. Am. Chem. Soc. 111,* 8551−8556.

Appelt, K., Bacquet, R. J., Barlett, C. A., Booth, C. L. J., Freer, S. T., Fuhry, M. A. M., Gehring, M. R., Herrmann, S. M., Howland, E. F., Janson, C. A., Jones, T. R., Kan, C. C., Kathardekar, V., Lewis, K. K., Marzoni, G. P., Matthews, D. A., Mohr, C., Moomaw, E. W., Morse, C. A., Oatley, S. J., Ogden, R. C., Reddy, M. R., Reich, S. H., Schoettlin, W. S., Smith, W. W., Varney, M. D., Villafranca, J. E., Ward, R. W., Webber, S., Webber, S. E., Welsh, K. M., & White, J. (1991) *J. Med. Chem. 34,* 1925−1934.

Åquist, J. (1990) *J. Phys. Chem. 94,* 8021−8024.

Atkins, W. M., & Sligar, S. G. (1988) *J. Biol. Chem. 263,* 18842−18849.

Badger, J., Minor, I., Kremer, M. J., Oliveira, M. A., Smith, T. J., Griffith, J. P., Guerin, D. M. A., Krishnaswamy, S., Luo, M., Rossmann, M., McKinlay, M. A., Diana, G. D., Dutko, F. J., Fancher, M., Rueckert, R. R., & Heinz, B. A. (1988) *Proc. Natl. Acad. Sci. U.S.A. 85,* 3304−3308.

Baldwin, J. E., Morris, G. M., & Richards, W. G. (1991) *Proc. R. Soc. London, Ser. B 245,* 43−51.

Baldwin, R. L. (1986) *Proc. Natl. Acad. Sci. U.S.A. 83,* 8069−8072.

Berendsen, H. J. C., Postma, J. P. M., van Gunsteren, W. V., Di Nola, A., & Haak, J. R. (1984) *J. Chem. Phys. 81,* 3684−3690.

Berendsen, H. J. C., Grigera, J. R., & Straatsma, T. P. (1987) *J. Phys. Chem. 91,* 6269−6271.

Bernstein, F. C., Koetzle, T. F., Williams, G. J. B., Smith, E. F. M. J., Brice, M. D., Rodgers, J. R., Kennard, O., Shimanouchi, T., & Tasumi, T. (1977) *J. Mol. Biol. 112,* 535−542.

Besler, B. H., Merz, K. M., & Kollman, P. A. (1990) *J. Comput. Chem. 11,* 431−439.

Bigler, T. L., Lu, W., Park, S. J., Tashiro, M., Wieczorek, M., Wynn, R., & Laskowski, M., Jr. (1993) *Protein Sci. 2,* 786−799.

Boobbyer, D. N. A., Goodford, P. J., McWhinnie, P. M., & Wade, R. C. (1989) *J. Med. Chem. 32,* 1083−1094.

Burmeister, W. P., Ruigrok, R. W. H., & Cusack, S. (1992) *EMBO J. 11,* 49−56.

Chan, H. S., & Dill, K. A. (1994) *J. Chem. Phys. 101,* 7007−7026.

Cherfils, J., & Janin, J. (1993) *Curr. Opin. Struct. Biol. 3,* 265−269.

Collins, J. R., Camper, D. L., & Loew, G. H. (1991) *J. Am. Chem. Soc. 113,* 2736−2743.

Colman, P. M. (1994) *Curr. Opin. Struct. Biol. 4,* 868−874.

Connelly, P. R., Aldape, R. A., Bruzzese, F. J., Chambers, S. P., Fitzgibbon, M. J., Fleming, M. A., Itoh, S., Livingston, D. J., Navia, M. A., Thomson, J. A., & Wilson, K. P. (1994) *Proc. Natl. Acad. Sci. U.S.A. 91,* 1964−1968.

Cramer, C. J., & Truhlar, D. G. (1992) *Science 256,* 213−217.

Cramer, C. J., Hawkins, G. D., Lynch, G. C., Giesen, D. J., Rossi, I., Storer, J. W., Truhlar, D. G., & Liotard, D. A. (1995) AMSOL version 5.0, QCPE Program 606.

Cupp-Vickery, J. R., & Poulos, T. L. (1995) *Nature, Struct. Biol. 2,* 144−152.

Datin, M. P. (1916) *Ann. Phys. 5,* 218−240.

De Voss, J. J., & Ortiz de Montellano, P. R. (1995) *J. Am. Chem. Soc. 117,* 4185−4186.

Dewar, M. J. S., & Thiel, W. (1977) *J. Am. Chem. Soc. 99,* 4899−4906.

Di Primo, C., Hui Bon Hoa, G., Douzou, P., & Sligar, S. (1990) *J. Biol. Chem. 265,* 5361−5363.

Di Primo, C., Hui Bon Hoa, G., Douzou, P., & Sligar, S. G. (1992) *Eur. J. Biochem. 209,* 583−588.

Di Primo, C., Hui Bon Hoa, G., Deprez, E., Douzou, P., & Sligar, S. G. (1993) *Biochemistry 32,* 3671−3676.

Di Primo, C., Deprez, E., Hui Bon Hoa, G., & Douzou, P. (1995) *Biophys. J. 68,* 2056−2061.

Eriksson, A. E., Baase, W. A., Zhang, X. J., Heinz, D. W., Blaber, M., Baldwin, E. P., & Matthews, B. W. (1992a) *Science 255,* 178−183.

Eriksson, A. E., Baase, W. A., Wozniak, J. A., & Matthews, B. W. (1992b) *Nature 355,* 371−373.

Ernst, J. A., Clubb, R. T., Zhou, H. X., Gronenborn, A. M., & Clore, G. M. (1995) *Science 267,* 1813−1817.

Fersht, A. R., Shi, J. P., Knill-Jones, J., Lowe, D. M., Wilkinson, A. J., Blow, D. M., Brick, P., Carter, P., Waye, M. M. Y., & Winter, G. (1985) *Nature 314,* 235−238.

Fisher, M. T., & Sligar, S. G. (1985) *J. Am. Chem. Soc. 107,* 5018−5019.

Fisher, M. T., & Sligar, S. G. (1987) *Biochemistry 26,* 4797−4803.

Fisher, M. T., Scarlata, S. F., & Sligar, S. G. (1985) *Arch. Biochem. Biophys. 240,* 456−463.

Fitzgerald, M. M., Churchill, M. J., McRee, D. E., & Goodin, D. B. (1994) *Biochemistry 33,* 3807−3818.

Fremont, D. H., Matsumura, M., Stura, E. A., Peterson, P. A., & Wilson, I. A. (1992) *Science 257,* 919−927.

Gao, J., Qiao, S., & Whitesides, G. M. (1995) *J. Med. Chem. 38,* 2292−2301.

Gaussian 92, Revision A (1992) Frisch, M. J., Trucks, G. W., Head-Gordon, M., Gill, P. M. W., Wong, M. W., Foresman, J. B., Johnson, B. G., Schlegel, H. B., Robb, M. A., Replogle, E. S., Gomperts, R., Andres, J. L., Raghavachari, K., Binkley, J. S., Gonzalez, C., Martin, R. L., Fox, D. J., Defrees, D. J., Baker, J., Stewart, J. J. P., & Pople, J. A. Gaussian, Inc., Pittsburgh, PA.

Goodford, P. J. (1985) *J. Med. Chem. 28,* 849−857.

Greer, J., Erickson, J. W., Baldwin, J. J., & Varney, M. D. (1994) *J. Med. Chem. 37,* 1035−1054.

Griffin, B. W., & Peterson, J. A. (1972) *Biochemistry 11,* 4740−4746.

Guengerich, F. P. (1991) *J. Biol. Chem. 266,* 10019−10022.

Gunsalus, I. C., & Wagner, G. C. (1978) *Methods Enzymol. 52,* 166−188.

Harris, D., & Loew, G. (1995) *J. Am. Chem. Soc. 117,* 2738−2746.

Helms, V., & Wade, R. (1995) *Biophys. J. 69,* 810−824.

Hui Bon Hoa, G., Douzou, P., Dahan, N., & Balny, C. (1982) *Anal. Biochem. 120,* 125−135.

Ishizaka, N. (1914) *Naunyn-Schmiedebergs Arch. Exp. Pathol. Pharmakol. 75,* 194−229.

Jackson, R. M., & Sternberg, M. J. E. (1994) *Protein Eng. 7,* 371−383.

Jones, J. P., Shou, M., & Korzekwa, K. R. (1995) *Biochemistry 34,* 6956−6961.

Jung, C., Ristau, O., & Rein, H. (1991) *Biochim. Biophys. Acta 1076,* 130−136.

Kauzmann, W. (1959) *Adv. Protein Chem. 14,* 1−63.

Kollman, P. A. (1993) *Chem. Rev. 93,* 2395−2417.

Kuntz, I. D. (1992) *Science 257,* 1078−1082.

Kuntz, I. D., Blaney, J. M., Oatley, S. J., Langridge, R., & Ferrin, T. E. (1982) *J. Mol. Biol. 161,* 269−288.

Loida, P. J., Sligar, S. G., Paulsen, M. D., Arnold, G. E., & Ornstein, R. L. (1995) *J. Biol. Chem. 270,* 5326−5330.
Lumry, R., & Rajender, S. (1970) *Biopolymers 9,* 1125−1227.
Mancera, R. L., & Buckingham, A. D. (1995) *Chem. Phys. Lett. 234,* 296−303.
Meerwein, H., & Gerard, L. (1923) *Annalen 435,* 174−189.
Murphy, K. P., Freire, E., & Paterson, Y. (1995) *Proteins 21,* 83−90.
Murray-Rust, P., & Glusker, J. P. (1984) *J. Am. Chem. Soc. 106,* 1018−1025.
Navia, M. A., & Murcko, M. A. (1992) *Curr. Opin. Struct. Biol. 2,* 202−210.
Nicholls, A., & Honig, B. (1991) *J. Comput. Chem. 12,* 435−445.
Otting, G., Liepinsh, E., & Wuethrich, K. (1991) *Science 254,* 974−980.
Pearlman, D. A., & Connelly, P. R. (1995) *J. Mol. Biol. 248,* 696−717.
Pisabarro, M. T., Ortiz, A. R., Palomer, A., Cabre, F., Garcia, L., Wade, R. C., Gago, F., Mauleon, D., & Carganico, G. (1994) *J. Med. Chem. 37,* 337−341.
Poulos, T. L., & Howard, A. J. (1987) *Biochemistry 26,* 8165−8174.
Poulos, T. L., & Raag, R. (1992) *FASEB J. 6,* 674−679.
Poulos, T. L., Finzel, B. C., & Howard, A. J. (1986) *Biochemistry 25,* 5314−5322.
Poulos, T. L., Finzel, B. C., & Howard, A. J. (1987) *J. Mol. Biol. 195,* 687−700.
QUANTA Release 4.0 (1992) Molecular Simulation Inc., 200 Fifth Ave., Waltham, MA 02154.
Quiocho, F. A. (1991) *Curr. Opin. Struct. Biol. 1,* 922−933.
Raag, R., & Poulos, T. L. (1989) *Biochemistry 28,* 917−922.
Raag, R., & Poulos, T. L. (1991) *Biochemistry 30,* 2674−2684.
Ryckaert, J. P., Ciccotti, G., & Berendsen, H. J. C. (1977) *J. Comput. Phys. 23,* 327−341.
Saenger, W. (1987) *Annu. Rev. Biophys. Biophys. Chem. 16,* 93−114.
Sali, A., Veerapandian, B., Cooper, J. B., Foundling, S. I., Hoover, D. J., & Blundell, T. L. (1989) *EMBO J. 8,* 2179−2188.
Savage, H. F. J. (1993) *Top. Mol. Struct. Biol. 17,* 3−43
Schulze, H., Ristau, O., & Jung, C. (1994) *Eur. J. Biochem. 224,* 1047−1055.
Serrano, L., Kellis, J. T., Jr., Cann, P., Matouschek, A., & Fersht, A. R. (1992) *J. Mol. Biol. 224,* 783−804.
Shoichet, B. K., Stroud, R. M., Santi, D. V., Kuntz, I. D., & Perry, K. M. (1993) *Science 259,* 1445−1450.
Sligar, S. G. (1976) *Biochemistry 15,* 5399−5406.
Sligar, S. G., Filipovic, D., & Stayton, P. S. (1991) *Methods Enzymol. 206,* 31−49.
Straatsma, T. P., & McCammon, J. A. (1990) *J. Comput. Chem. 11,* 943−951.
Tanford, C. (1973) *The hydrophobic effect: formation of micelles and biological membranes*, Wiley, New York.
Tsai, R., Yu, C. A., Gunsalus, I. C., Peisach, J., Blumberg, W., Orme-Johnson, W. H., & Beinert, H. (1970) *Proc. Natl. Acad. Sci. U.S.A. 66,* 1157−1163.
van Gunsteren, W. F., & Berendsen, H. J. C. (1987) *Groningen Molecular Simulation (GROMOS) Library Manual*, Biomos, Nijenborgh 16, 9747 AG Groningen, The Netherlands.
Varghese, J. N., McKimm-Breschkin, J. L., Caldwell, J. B., Kortt, A. A., & Colman, P. M. (1992) *Proteins 14,* 327−332.
Verlinde, C. L. M. J., Callens, M., Van Calenbergh, S., Van Aerschot, A., Herdewijn, P., Hannaert, V., Michels, P. A. M., Opperdoes, F. R., & Hol, W. G. J. (1994) *J. Med. Chem. 37,* 3605−3613.
Vermersch, P. S., Lemon, D. D., Tesmer, J. J. G., & Quiocho, F. A. (1991) *Biochemistry 30,* 6861−6866.
Vriend, G., Berendsen, H. J. C., van der Zee, J. R., van den Burg, B., Venema, G., & Eijsink, V. G. H. (1991) *Protein Eng. 4,* 941−945.
Wade, R. C. (1990) *J. Comput. Aided Mol. Des. 4,* 199−204.
Wade, R. C., & Goodford, P. J. (1993) *J. Med. Chem. 36,* 148−156.
Wade, R. C., Clark, K. J., & Goodford, P. J. (1993) *J. Med. Chem. 36,* 140−147.
Weber, P. C., Wendolowski, J. J., Pantoliano, M. W., & Salemme, F. R. (1992) *J. Am. Chem. Soc. 114,* 3197−3200.
Weis, W., Brown, J. H., Cusack, S., Paulson, J. C., Skehel, J. J., & Wiley, D. C. (1988) *Nature 333,* 426−431.

BI951817L